Supplementary Information

Reduced 0.418 V V_{OC}-deficit of 1.73 eV wide-bandgap perovskite solar cells assisted by dual chlorides for efficient all-perovskite tandems

Yue Zhao,[‡][ab] Changlei Wang,[‡][*][ab] Tianshu Ma,[ab] Luwei Zhou,[ab] Zhanghao Wu,[ab] Huayang Wang,[ab] Cong Chen,[c] Zhenhua Yu,[d] Weiwei Sun,[e] Aolin Wang,[f] Hao Huang,[f] Bingsuo Zou,[f] Dewei Zhao[*][c] and Xiaofeng Li[*][ab]

[a] *School of Optoelectronic Science and Engineering & Collaborative Innovation Center of Suzhou Nano Science and Technology, Soochow University, Suzhou 215006, China*
E-mail: cl.wang@suda.edu.cn, xfli@suda.edu.cn
[b] *Key Lab of Advanced Optical Manufacturing Technologies of Jiangsu Province & Key Lab of Modern Optical Technologies of Education Ministry of China, Soochow University, Suzhou 215006, China*
[c] *College of Materials Science and Engineering, Engineering Research Center of Alternative Energy Materials & Devices, Ministry of Education, Sichuan University, Chengdu 610065, China*
E-mail: dewei_zhao@hotmail.com and dewei.zhao@scu.edu.cn
[d] *Key Laboratory of Artificial Micro- and Nano-structures of Ministry of Education of China, School of Physics and Technology, Wuhan University, Wuhan 430072, China*
[e] *College of Aerospace Science and Engineering, National University of Defense Technology, Changsha 410073, China*
[f] *Guangxi Key Laboratory of Processing for Non-ferrous Metals and Featured Materials, School of Resources, Environments and Materials, Guangxi University, Nanning 530004, China*
‡ These authors contributed equally.

Experimental Section

Materials

Phenmethylammonium chloride (PMACl, 99.9%), poly [(9,9-bis(3'-(N,N-dimethyl)-N-ethylammoinium-propyl)-2,7-fluorene)-alt-2,7-(9,9-dioctylfluorene)] dibromide (PFNBr, 98%), cesium iodide (CsI, 99.9%), formamidinium bromine (FABr, 99.9%), lead iodide (PbI_2, 99.9%), lead bromide ($PbBr_2$, 99.9%), lead chlorine ($PbCl_2$, 99.9%), poly (triarylamine) (PTAA, 99.9%), and ethane-1,2-diamine,dihydroiodide ($EDAI_2$, 99.5%) were purchased from Xi'an Polymer Light Technology Corp.. Formamidinium iodide (FAI, 99.9%) was purchased from Greatcell. C_{60} was purchased from Nano-C, bathocuproine (BCP) was purchased from Jilin OLED Company (China). Tin floride (SnF_2, 99%), N,N-dimethylformamide (DMF, anhydrous), dimethyl sulfoxide (DMSO, anhydrous), isopropanol (IPA, anhydrous), diethyl ether (anhydrous), chlorobenzene (CB, anhydrous), lead thiocyanate ($Pb(SCN)_2$, 99.5%) and kalium thiocyanate (KSCN, 99.5%) were purchased from Sigma-Aldrich. Poly(3,4-ethylenedioxythiophene): polystyrene sulfonate (PEDOT:PSS, CLEVIOS™ PVP AI 4083) was purchased from Heraeus, LLC. Indium tin oxide (ITO, In_2O_3/SnO_2 90/10 wt%) target, copper (Cu) and silver (Ag) were purchased from Kairui Xincai. All chemicals used in this work are commercially available and are used as received.

Preparation of wide-E_g perovskite precursors and films

The 1.73 eV $FA_{0.8}Cs_{0.2}Pb(I_{0.7}Br_{0.3})_3$ perovskite precursor solution was prepared by dissolving 0.5 mmol FAI, 0.2 mmol CsI, 0.3 mmol FABr, 0.7 mmol PbI_2 and 0.3 mmol $PbBr_2$ in 1 ml mixed solvent of DMF and DMSO with a volume ratio of 3:1. Then 4.85 mg $Pb(SCN)_2$ and 1 mg KSCN were added into the solution. The perovskite precursor solution was thoroughly mixed and aged for 12 hours before using. $PbCl_2$ stock solution was prepared by dissolving 0.5 mmol $PbCl_2$ in 500 μL DMSO. Then, 10 μL $PbCl_2$ solution was added into 1 mL control perovskite precursor to form the $PbCl_2$-based perovskite precursor. PMACl stock solution was prepared by dissolving 0.5 mmol PMACl in 500 μL DMSO, and 10 μL PMACl solution was further added into 1 mL control perovskite precursor solution to form the PMACl-based perovskite solution. For

PbCl$_2$+PMACl-based perovskite solution, 0.5 mmol PbCl$_2$ and 0.5 mmol PMACl were both added into 500 μL DMSO, and 10 μL of this stock solution was added into 1 mL control perovskite precursor solution to form the PbCl$_2$+PMACl co-modified perovskite precursor.

Wide-E_g perovskite film preparation: Wide-E_g perovskite layers with different additives were deposited through a two-step spin-coating process, i.e., 500 rpm for 2 s and 4000 rpm for 60 s, and the antisolvent of 700 μL diethyl ether was dripped at 25 s of the second step. The as-deposited film would be annealed at 65 ºC for 2 min and then 100 ºC for 10 min.

Preparation of low-E_g perovskite precursors and films

Low-E_g (FASnI$_3$)$_{0.6}$(MAPbI$_3$)$_{0.4}$ perovskite precursor: FASnI$_3$ precursor solution was prepared by dissolving 372 mg SnI$_2$ and 172 mg FAI with 5 mol% (7.8 mg) SnF$_2$ in mixed DMF and DMSO solution. MAPbI$_3$ precursor solution was prepared by dissolving 461 mg PbI$_2$ and 159 mg MAI with 3.5 mol% (11.3 mg) Pb(SCN)$_2$ in 565 μL DMF and 71 μL DMSO mixed solution. (FASnI$_3$)$_{0.6}$(MAPbI$_3$)$_{0.4}$ precursor solution was obtained by mixing stoichiometric amounts of FASnI$_3$ and MAPbI$_3$ perovskite precursors. The mixed solution was kept for 30 min before spin coating.

Low-E_g perovskite film: The low-E_g (FASnI$_3$)$_{0.6}$(MAPbI$_3$)$_{0.4}$ precursor was spin-coated on substrates at 4000 rpm for 60 s with 600 μL diethyl ether dripped simultaneously during the spinning. The as-deposited film would be annealed at 65 ºC for 3 min and then 100 ºC for 7 min.

Fabrication of single-junction PSCs and all-perovskite TSCs

Wide-E_g PSCs: The pre-patterned ITO substrates were cleaned through sonication in deionized water and ethanol sequentially, and then cleaned by UV/Ozone treatment (Jelight Company Inc.) for 20 min before using. PTAA dissolved in CB (4 mg/mL) was spin-coated onto the ITO substrates at 5000 rpm for 30 s and then dried at 100°C for 10 min, followed by being coated with an ultrathin layer of PFNBr. Wide-E_g perovskite layers were then quickly spin-coated on the PTAA layer with different precursors as

described above through a two-step process, i.e., 500 rpm for 2 s and 4000 rpm for 60 s, and the antisolvent of 700 μL diethyl ether was dripped at 25 s of the second step. Then, the samples were transferred into a vacuum chamber for the thermal evaporation of functional layers. C_{60} (20 nm)/BCP (5 nm)/Cu (100 nm) were sequentially deposited on the perovskite film to complete the solar cell fabrication.

Low-E_g PSCs: Sonication-cleaned ITO substrates were treated under UV-ozone for 20 min, and then 20 nm PEDOT:PSS layer was spin-coated on ITO, followed by being annealed at 150 °C for 20 min in ambient air. The substrates were then transferred into a N_2-filled glovebox for the deposition of perovskite films. $(FASnI_3)_{0.6}(MAPbI_3)_{0.4}$ perovskite precursors were spin-coated on the PEDOT:PSS layer at 1000 rpm for 10 s and 4000 rpm for 60 s. During the spin-coating, 600 μL diethyl ether was dropped on the film. The perovskite film was annealed as the same way mentioned above. After the deposition of perovskite layer, the samples were then put into a high vacuum chamber for the following deposition of functional layers. 20 nm C_{60} and 5 nm BCP were sequentially evaporated onto the perovskite. 100 nm Cu was finally deposited with an active area of 0.09 cm². At last, the devices were encapsulated with cover glass and UV-curable epoxy.

For 2T all-perovskite TSCs, the device structure is ITO/PTAA/PFNBr/wide-E_g perovskite/C_{60}/SnO$_2$/ITO/PEDOT:PSS/low-E_g perovskite/C_{60}/BCP/Cu. The wide-E_g perovskite top subcell was fabricated using the same method as mentioned above. The interconnecting layer is SnO$_2$/ITO, where 20 nm SnO$_2$ was formed using atomic layer deposition (ALD) at 70 °C, and the 100 nm ITO layer was deposited by magnetron sputtering at 60 W for 20 min. Following deposition of low-E_g bottom subcell used the same method as described above. At last, the devices were encapsulated with cover glass and UV-curable epoxy.

Film and device characterization

The microscopic morphologies were characterized by a field emission scanning electron microscope (SEM, ZEISS, Sigma 300). The optical properties, including absorbance, transmittance and reflectance spectra, were all measured by an UV-vis-

NIR spectrometer (PekinElmer, Lambda 1050 S+). The XRD patterns were obtained by using a Bruker D8 advance diffractometer. XPS was performed using a micro-focus monochromatic Al Kα–ray source (Thermo Scientfic Escalab 250Xi US), which corresponded to the instrument resolution of 0.45 eV that was determined by the Ag $3d_{5/2}$ peak. PL and TRPL measurements were performed on perovskite films directly deposited on glasses using flashing light system (FLS980, Edinburgh Inc.). ToF-SIMS measurements were performed on a ToF-SIMS.5 instrument from IONTOF, Germany, operated in spectral mode using a 30 keV Bi^{3+} primary ion beam. For depth profiling, a 1000 eV O^{2+} sputter beam was used to remove the material layer-by-layer in interlaced mode from a raster area of 300×300 μm^2. Negative ions were collected for depth profile analysis. The mass-spectrometry was performed on an area of 115×115 μm^2 in the center of the sputter crater.

J-V curves were measured in air under 100 mW/cm^2 AM 1.5G solar irradiation (SS-F5-3A, Enlitech) with a Keithley 2400 sourcemeter. The light intensity for J-V measurements was calibrated by a standard Si solar cell. The steady-state power outputs of PSCs and TSCs were obtained by tracking the maximum power point under constant illumination (100 mW/cm^2) with a LED source, and the devices were kept in inert condition without encapsulation and temperature control units. The dark current was recorded with a semiconductor parameter analyzer (Agilent, B1500A). EQE spectra were performed from 300 nm to 1100 nm on a QE system (QE-R, Enlitech). For the EQE measurements of TSCs, a white light was used as the external light source with the 550 and 850 nm filters for bottom and top subcells, respectively. SCLC measurements were conducted by using a semiconductor parameter analyzer (Agilent, B1500A) with the voltage swept from -0.1 V to 3 V. For EIS characterizations and C-V measurements, an electrochemical workstation (CIMPS, Zennium Zahner) was used under dark condition.
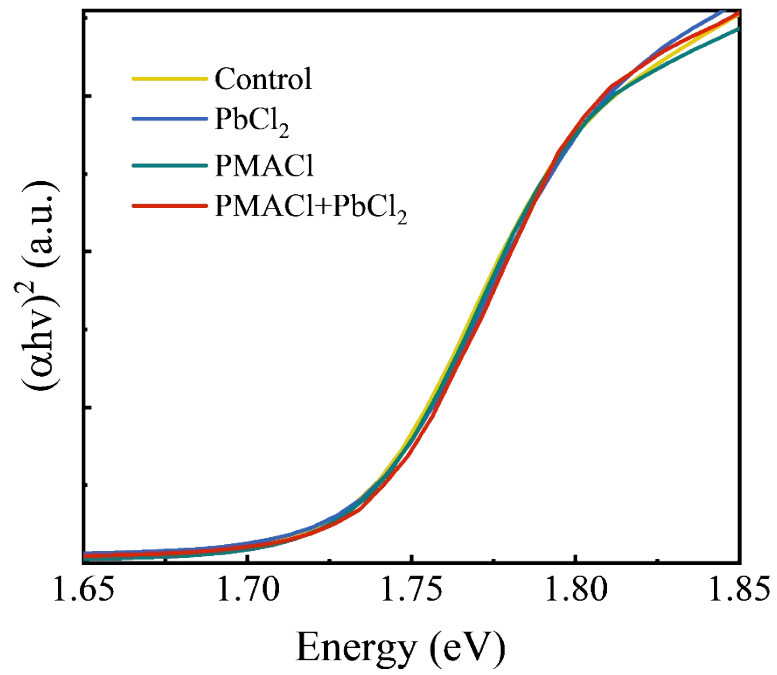
Fig. S1 Tauc plots of wide-E_g perovskite films with different additives (control, $PbCl_2$, PMACl, and $PbCl_2$+PMACl).
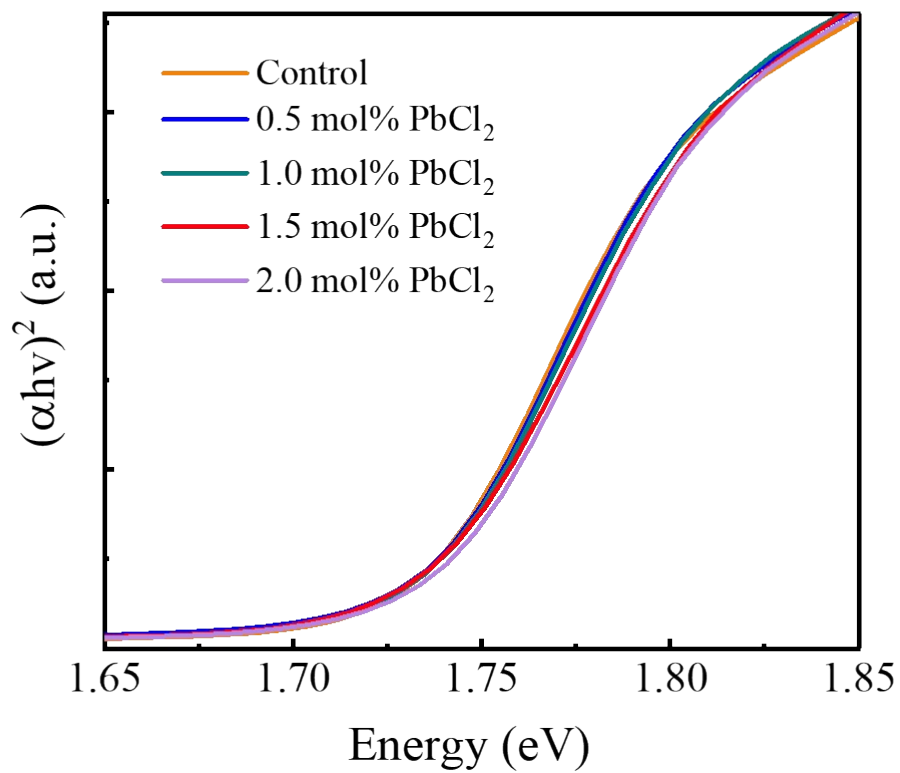
Fig. S2 Tauc plots of wide-E_g perovskite films with $PbCl_2$ concentration changing from 0 to 2.0 mol%.
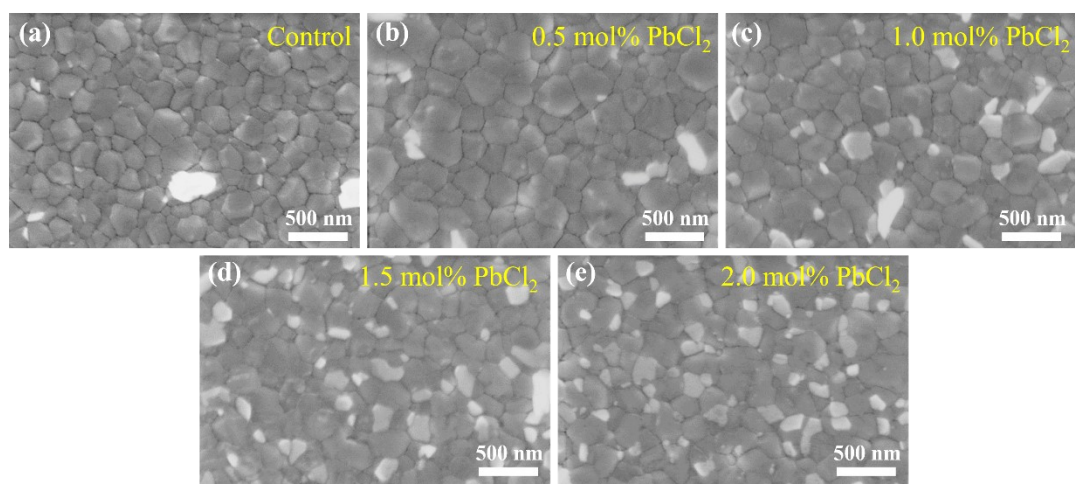
Fig. S3 Top-view SEM images of wide-E_g perovskite films treated with different concentrations of PbCl$_2$: (a) Control, (b) 0.5 mol%, (c) 1.0 mol%, (d) 1.5 mol%, and (e) 2.0 mol%.
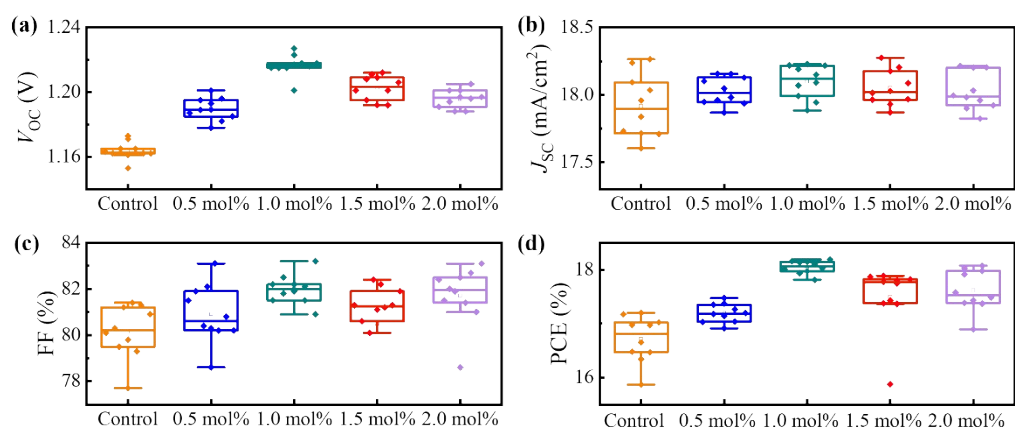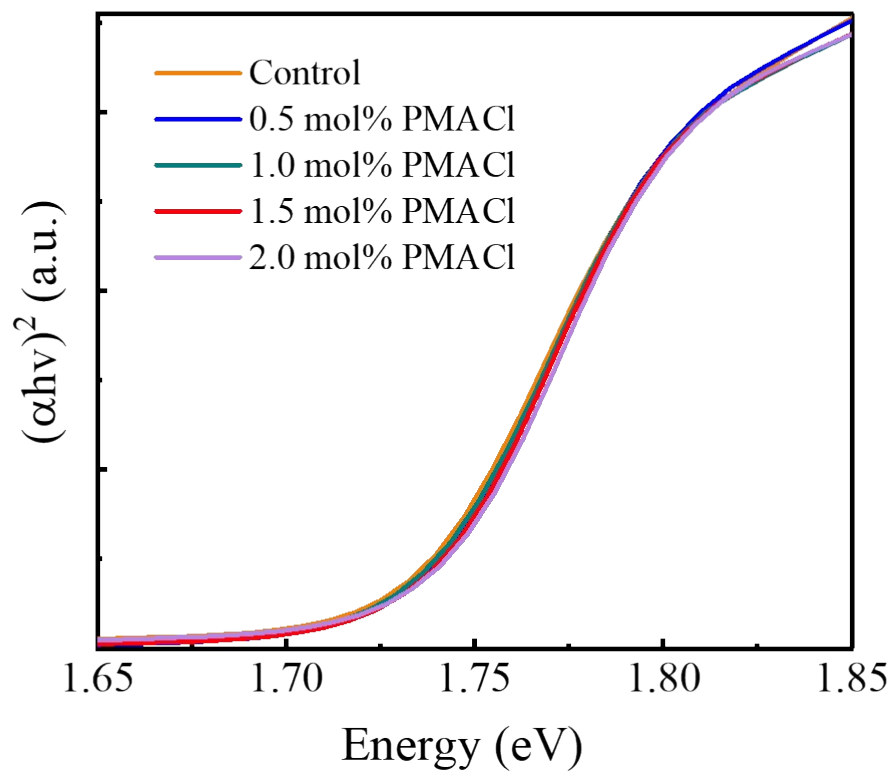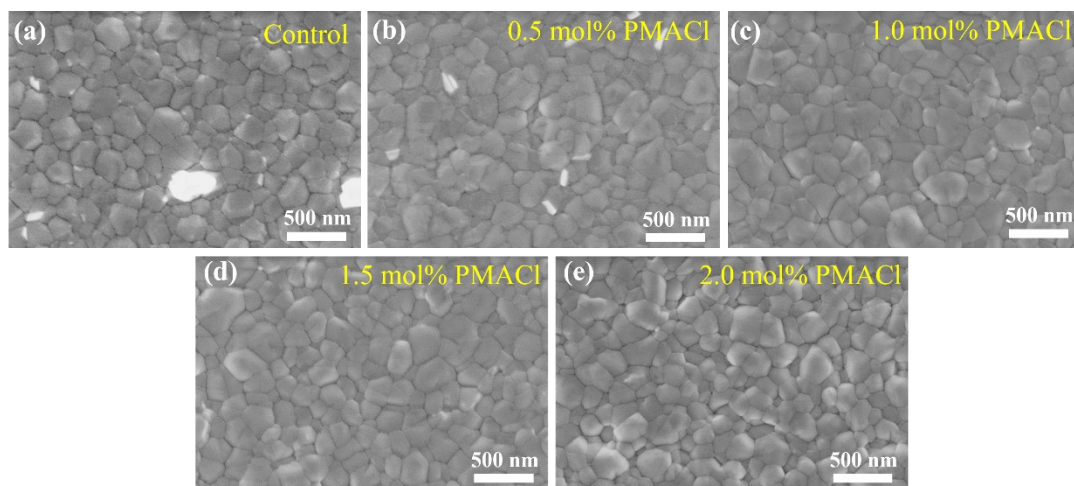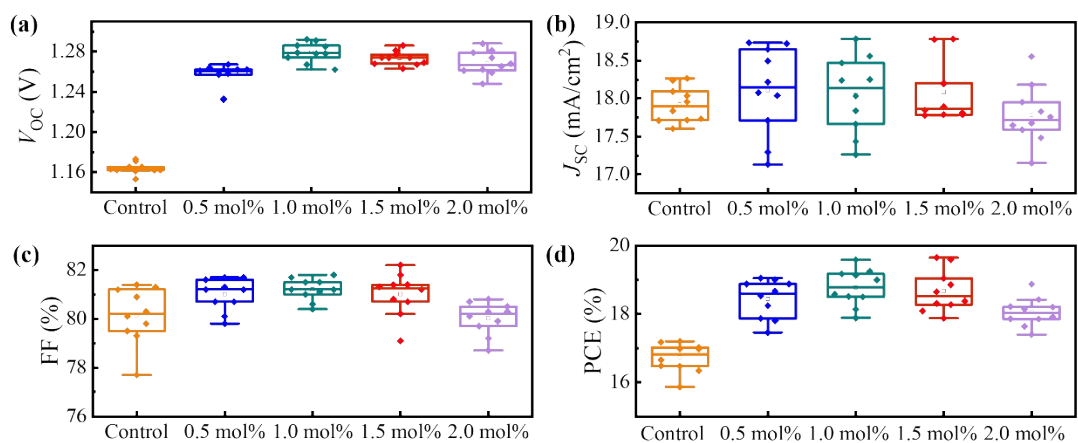
Fig. S4 Statistical results of (a) V_{OC}, (b) J_{SC}, (c) FF, and (d) PCE of wide-E_g PSCs with PbCl$_2$ concentration changing from 0 to 2.0 mol%. These results are calculated from 50 individual devices.

Fig. S5 Tauc plots of wide-E_g perovskite films with PMACl concentration changing from 0 to 2.0 mol%.

Fig. S6 Top-view SEM images of wide-E_g perovskite films treated with different concentrations of PMACl: (a) Control, (b) 0.5 mol%, (c) 1.0 mol%, (d) 1.5 mol%, and (e) 2.0 mol%.

Fig. S7 Statistic results of (a) V_{OC}, (b) J_{SC}, (c) FF, and (d) PCE of wide-E_g PSCs with PMACl concentration changing from 0 to 2.0 mol%. These results were calculated from 50 individual devices.
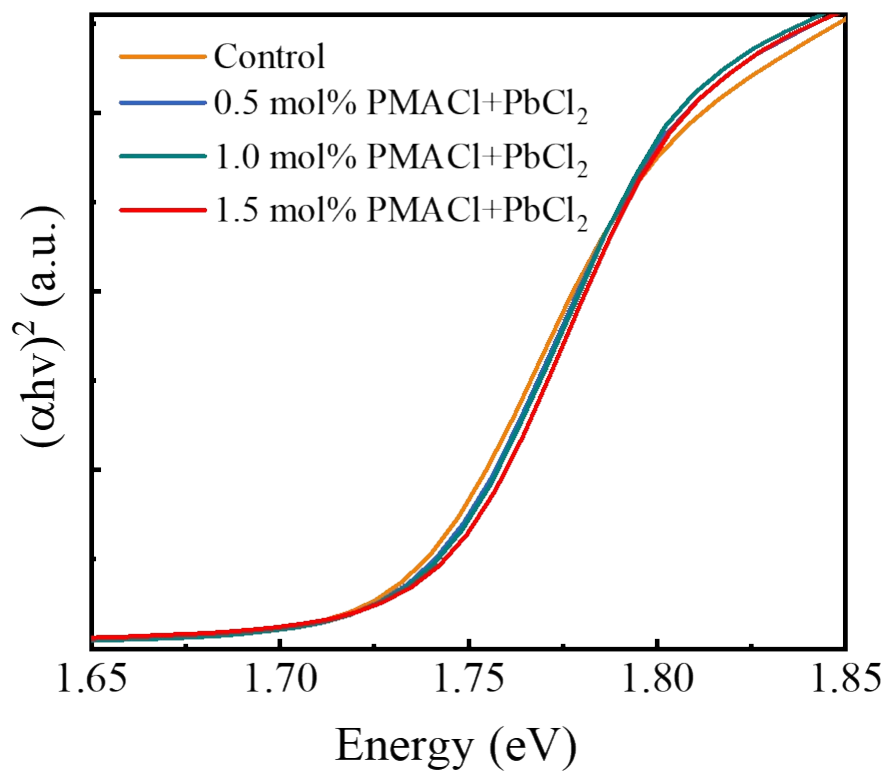
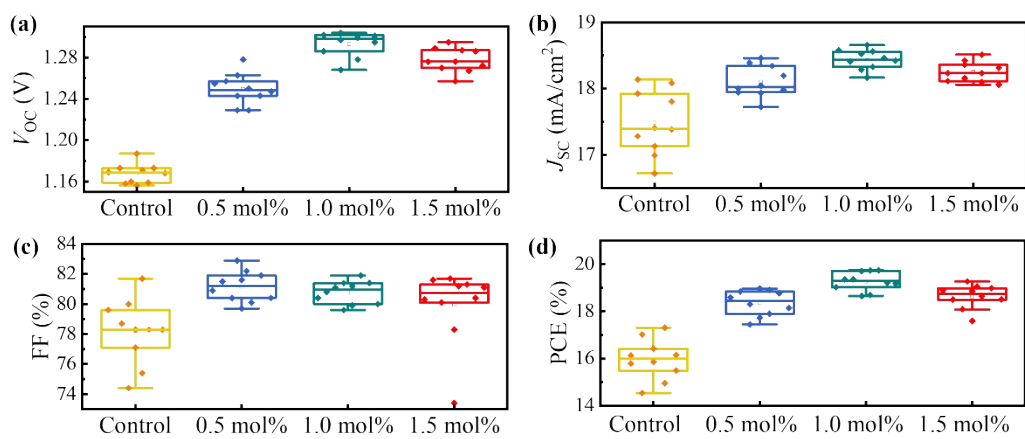**Fig. S8** Tauc plots of wide-E_g perovskite films with different $PbCl_2$+PMACl concentrations.

Fig. S9 Statistic results of (a) V_{OC}, (b) J_{SC}, (c) FF, and (d) PCE of wide-E_g PSCs with different PbCl$_2$+PMACl concentrations. These results were calculated from 40 individual devices.
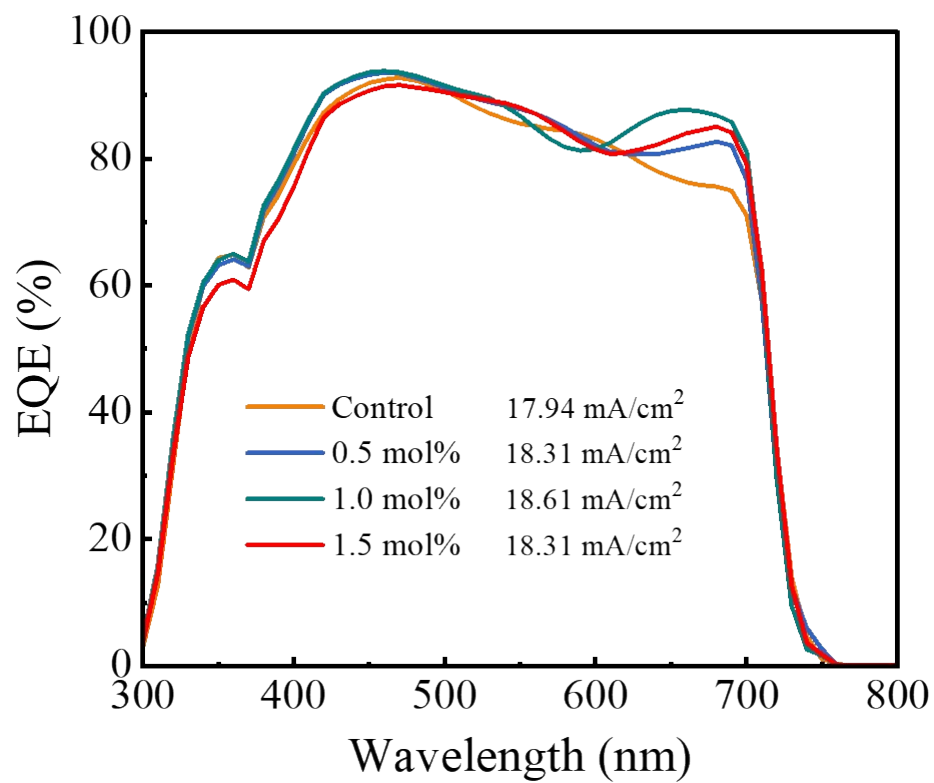
Fig. S10 EQE plots of wide-E_g PSCs with different PbCl$_2$+PMACl concentrations (Control, 0.5 mol%, 1.0 mol%, and 1.5 mol%).
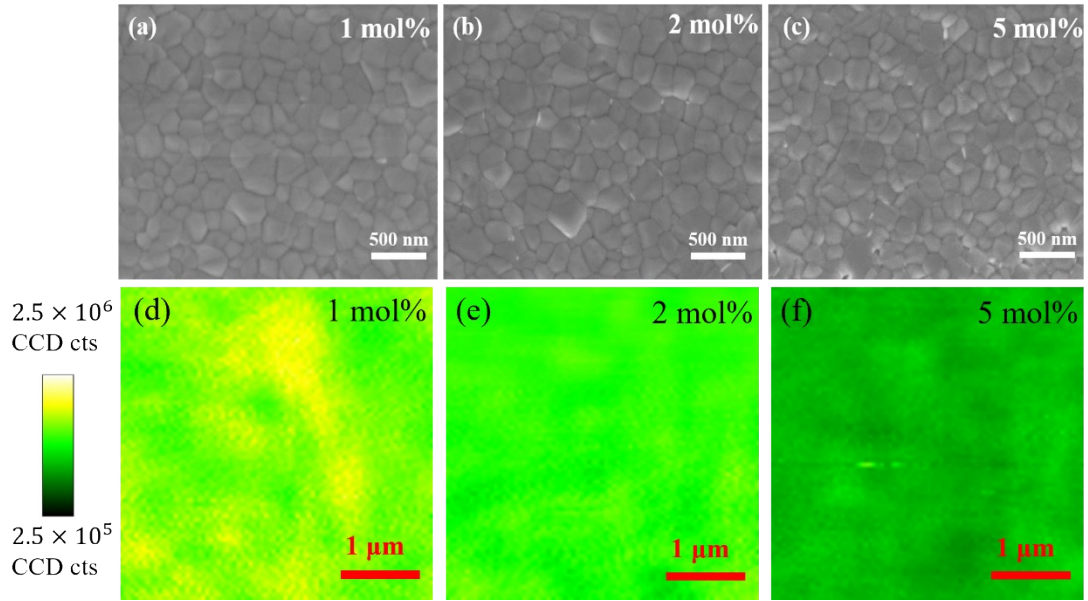
Fig. S11 (a-c) Top-view SEM images and (d-f) PL mapping images of wide-E_g perovskite films with high $PbCl_2$+PMACl concentrations: (a, d) 1 mol%, (b, e) 2 mol%, and (c, f) 5 mol%.
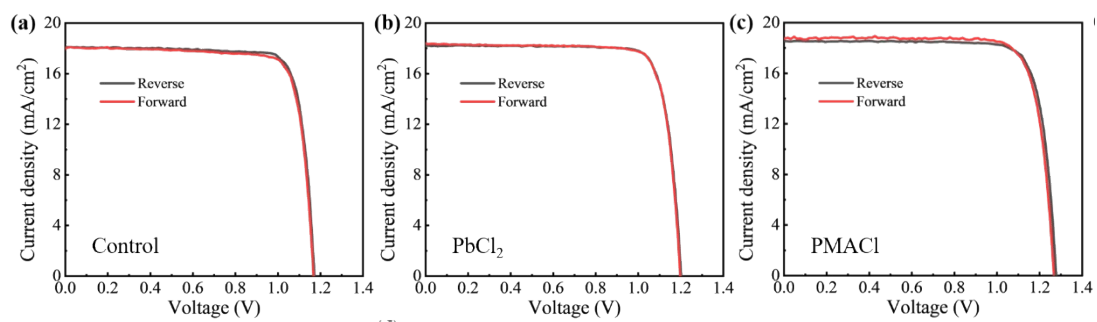
Fig. S12 *J-V* curves under reverse and forward voltage scans of the best performing (a) control, (b) PbCl$_2$, and (c) PMACl wide-E_g PSCs.
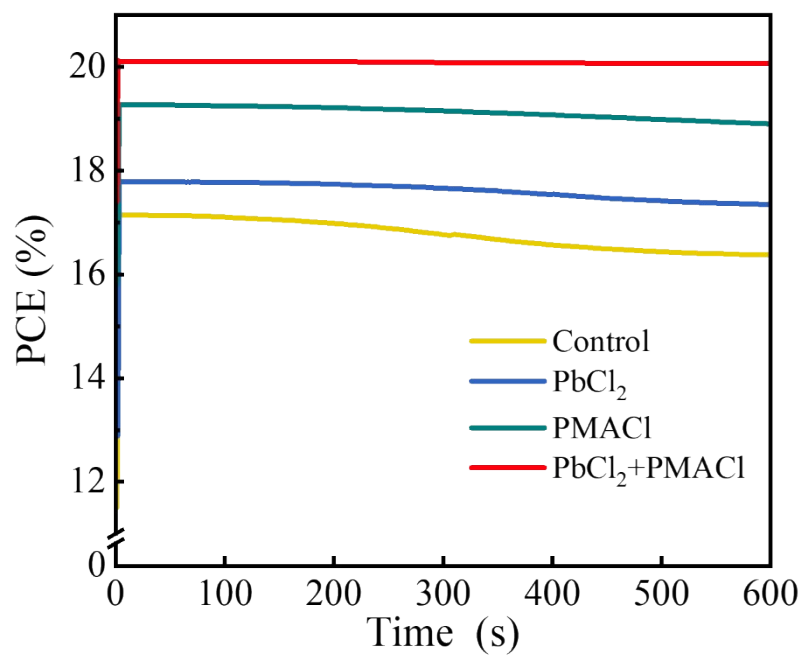
Fig. S13 Power outputs of control, PbCl$_2$, PMACl, and PbCl$_2$+PMACl wide-E_g PSCs measured by using MPP tracking. The unencapsulated cells were measured under AM 1.5G in the inert condition.
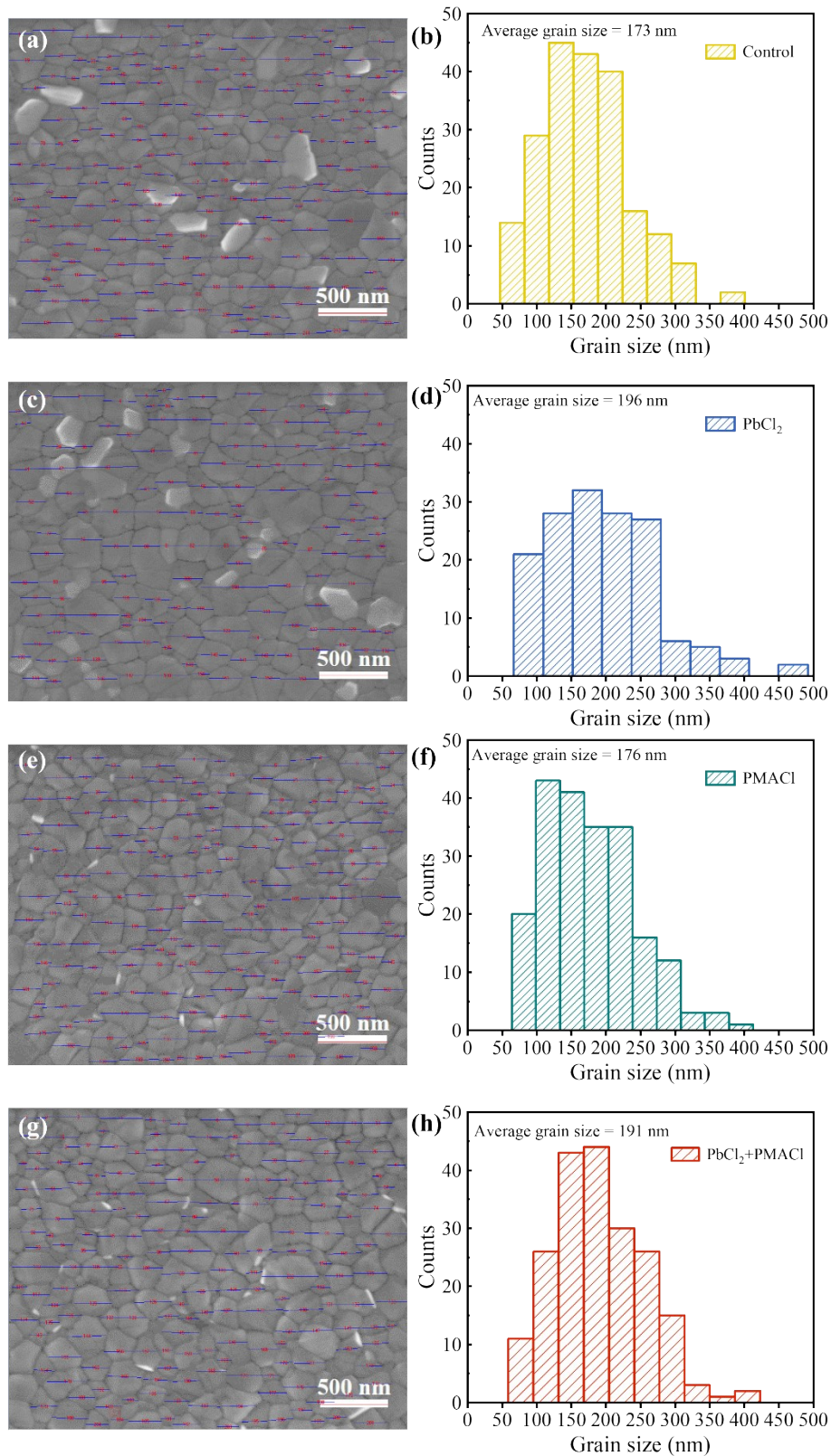
Fig. S14 Statistics of grain size for perovskite films based on (a) control, (c) PbCl$_2$, (e) PMACl and (g) PbCl$_2$+PMACl, and the corresponding grain size distribution of perovskite films based on (b) control, (d) PbCl$_2$, (f) PMACl, and (h) PbCl$_2$+PMACl.

Control	**PbCl$_2$+PMACl**

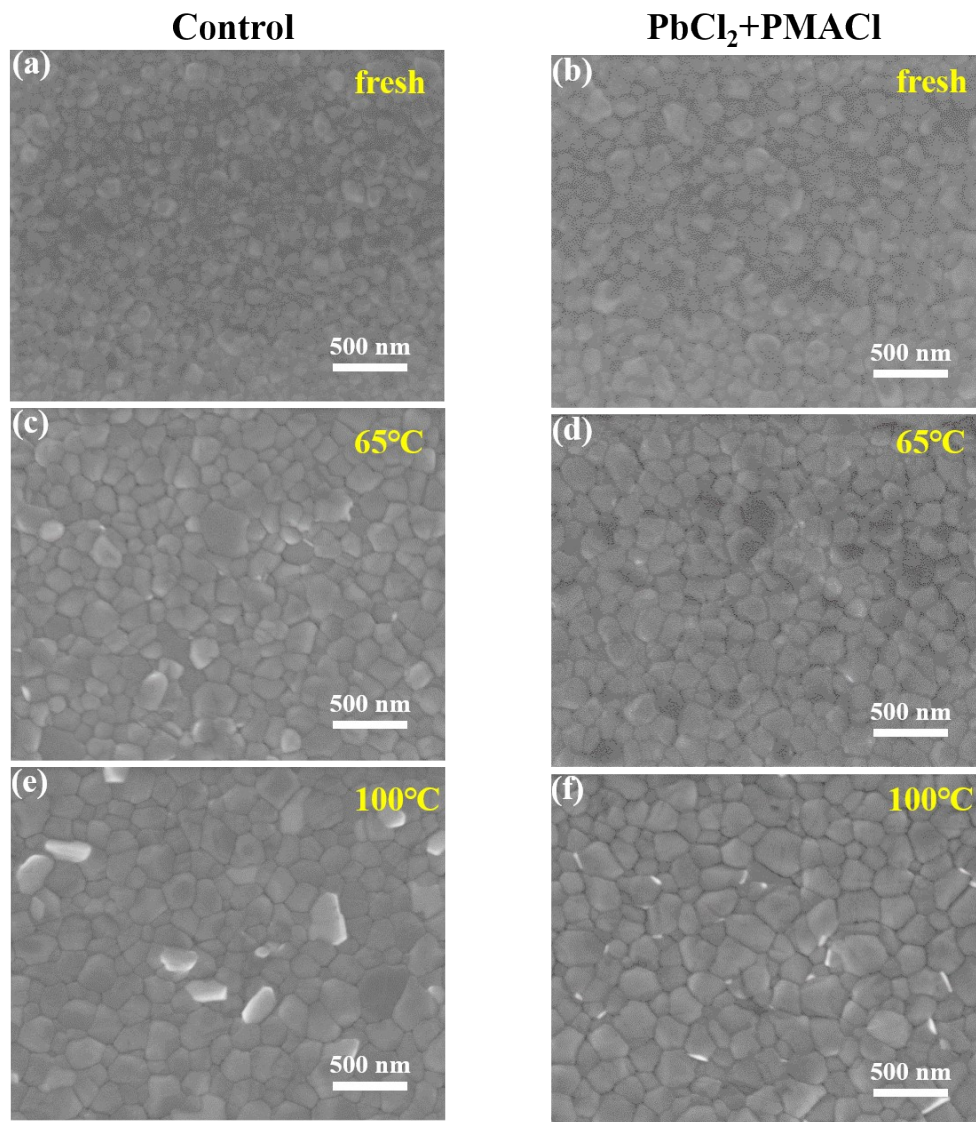**Fig. S15** Top-view SEM images of control and PbCl$_2$+PMACl wide-E_g perovskite films at different annealing temperature: (a, b) fresh, (c, d) 65 °C for 10 mins, (e, f) 100 °C for 10 mins.

(a)

RMS=32.8 nm

(b)

RMS=35.9 nm

(c)

RMS=18.5 nm

(d)

RMS=26 nm

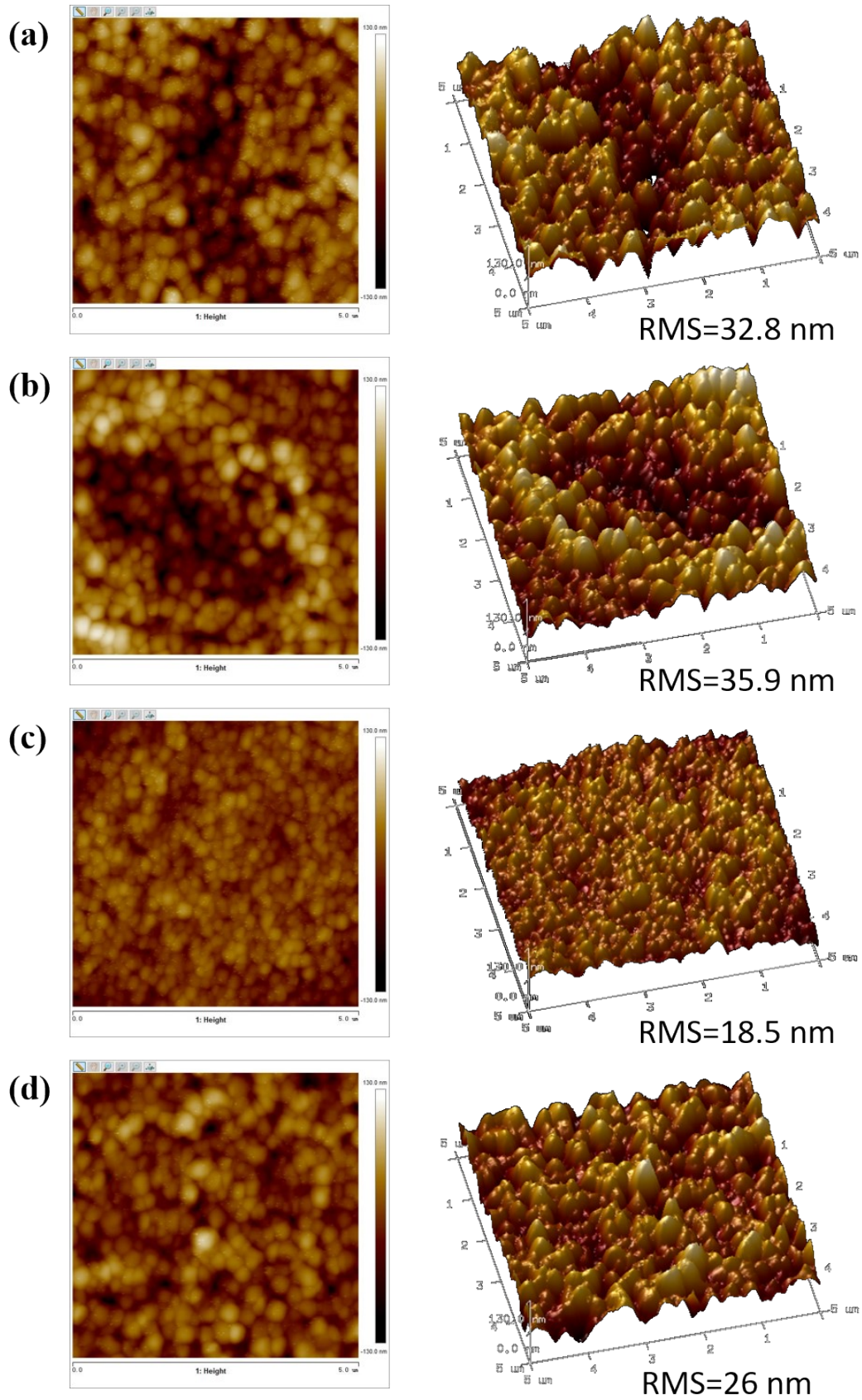**Fig. S16** AFM images of (a) control, (b) $PbCl_2$, (c) PMACl, and (d) $PbCl_2$+PMACl wide-E_g perovskite films.
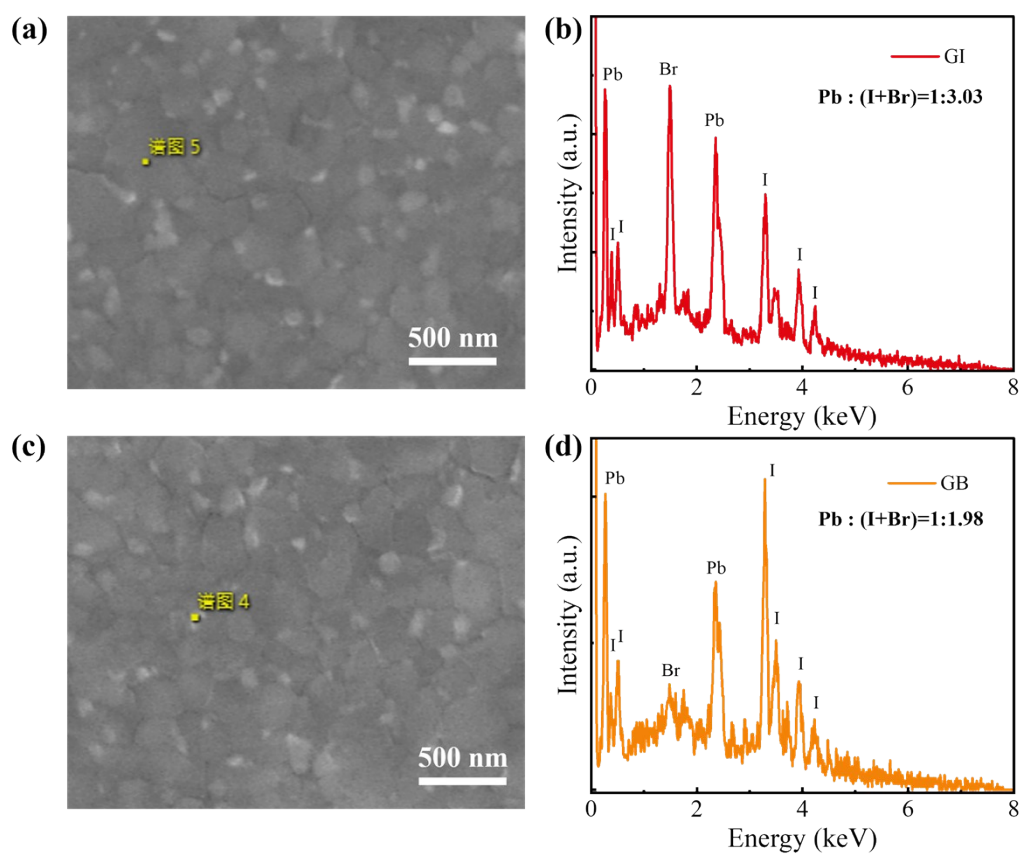
Fig. S17 Top-view SEM images and corresponding EDS spectra of $PbCl_2$ only wide-E_g perovskite films taken from (a, b) a grain interior and (c, d) a bright part at the grain boundary.
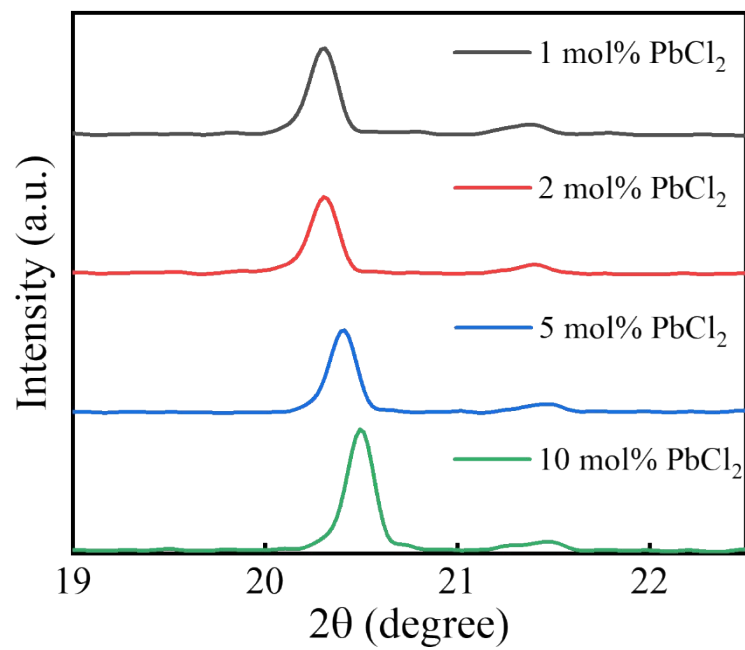
Fig. S18 XRD patterns of wide-E_g perovskite films treated with different concentrations of $PbCl_2$, where 2θ ranges from 19º to 22.5º.
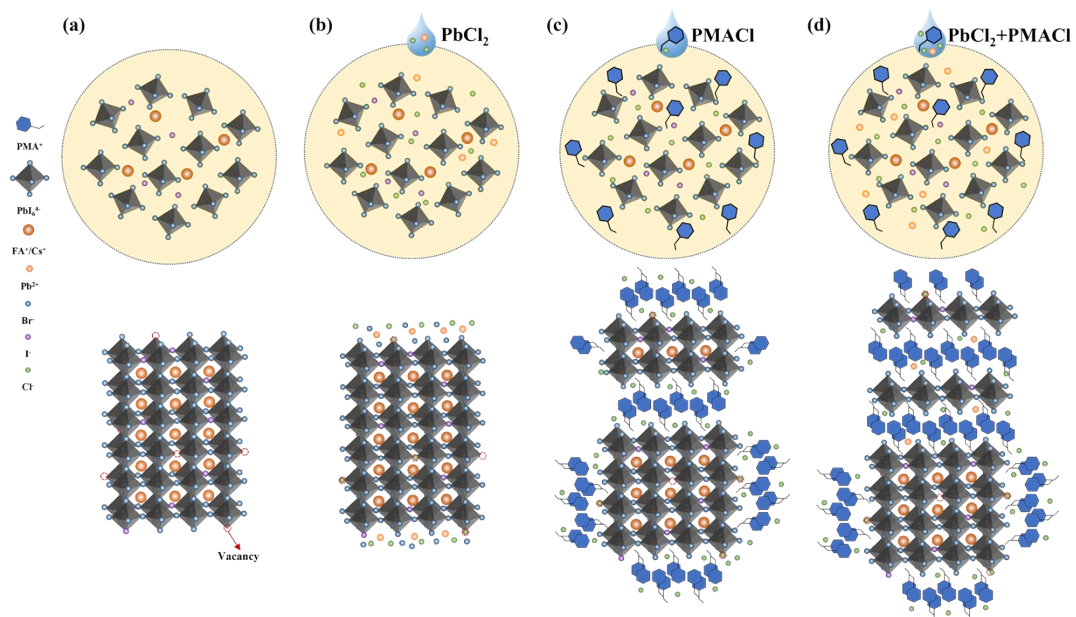
Fig. S19 Schematic of perovskite films treated by (b) PbCl$_2$, (c) PMACl and (d) PbCl$_2$+PMACl, while (a) is the control film.
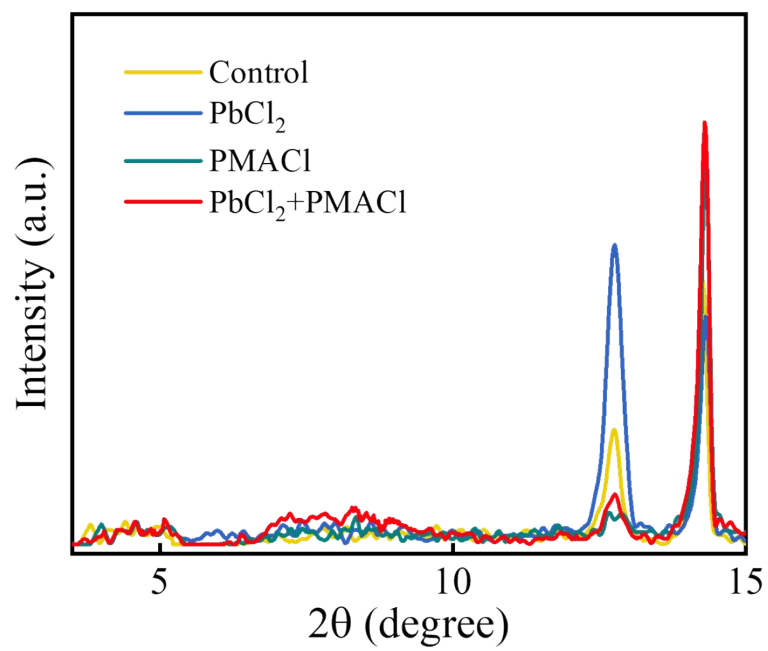
Fig. S20 XRD patterns of control, $PbCl_2$, PMACl, and $PbCl_2$+PMACl treated perovskite films, where 2θ ranges from 3.5º to 15º.
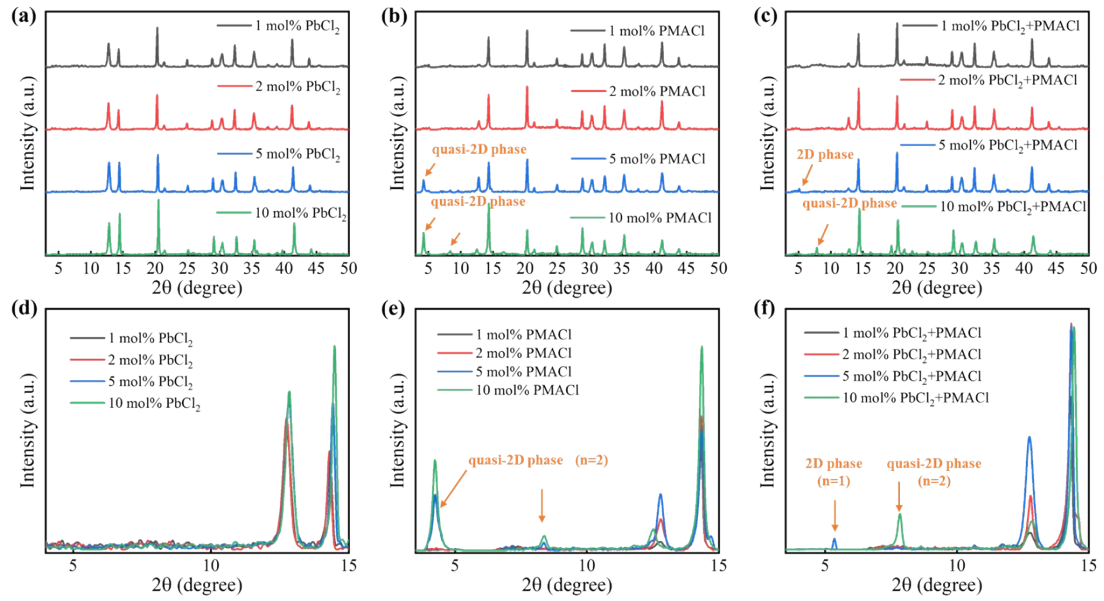
Fig. S21 XRD patterns of wide-E_g perovskite films treated with different concentrations of (a, d) $PbCl_2$, (b, e) PMACl, and (c, f) $PbCl_2$+PMACl. Full 2θ range in (a-c) is from 3.5º to 50º, and the range is narrowed from 3.5º to 15º in (d-f).
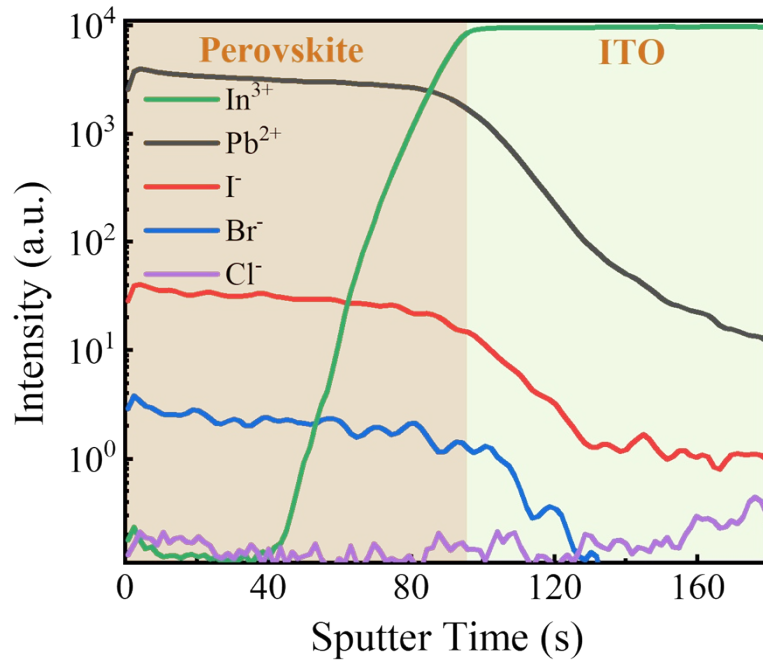
Fig. S22 ToF-SIMS profiles of the control perovskite film. No Cl distribution can be found in the film.
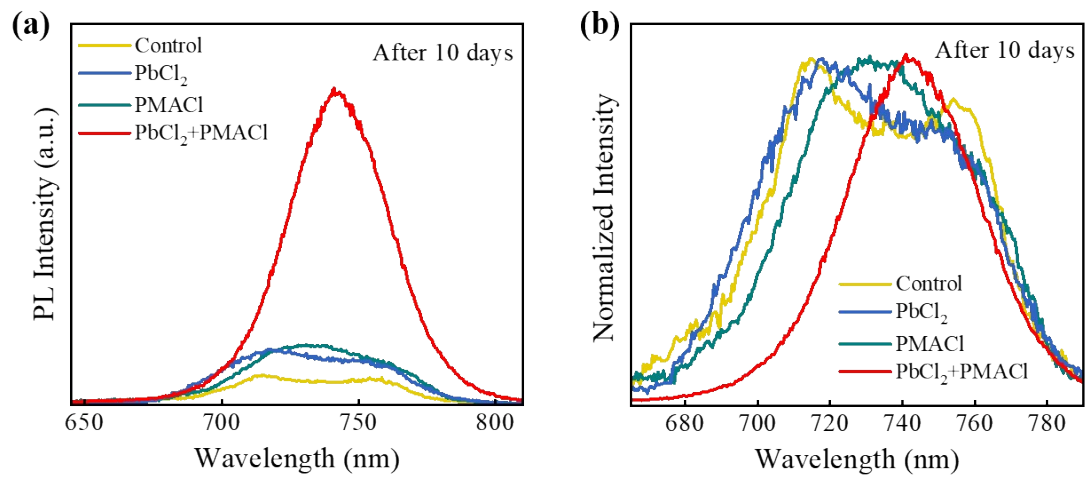
Fig. S23 PL spectra of control, PbCl$_2$, PMACl and PbCl$_2$+PMACl treated perovskite films. These wide-E_g samples have been aged for 10 days in inert condition. (a) Absolute PL intensity spectra, (b) normalized PL intensity spectra.
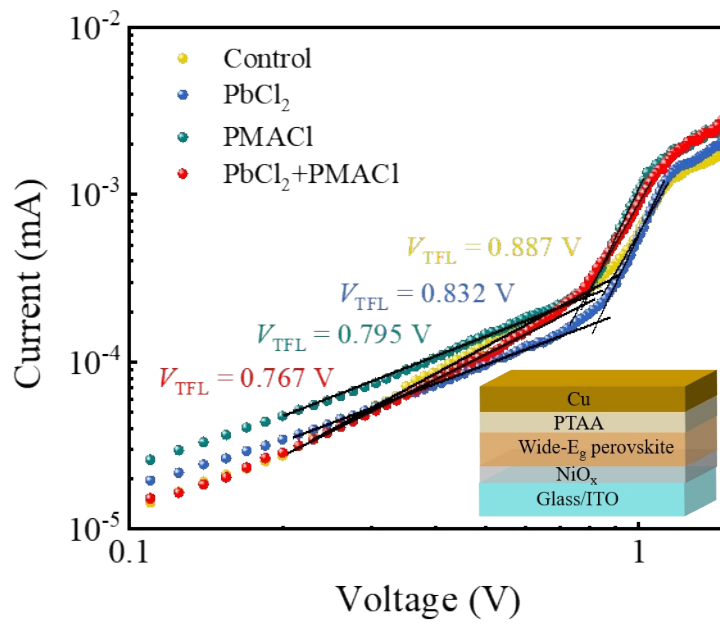
Fig. S24 SCLC measurements of the hole-only devices with a structure of ITO/NiO$_x$/wide-E_g perovskite/PTAA/Cu for different perovskite films (control, PbCl$_2$, PMACl, and PbCl$_2$+PMACl).
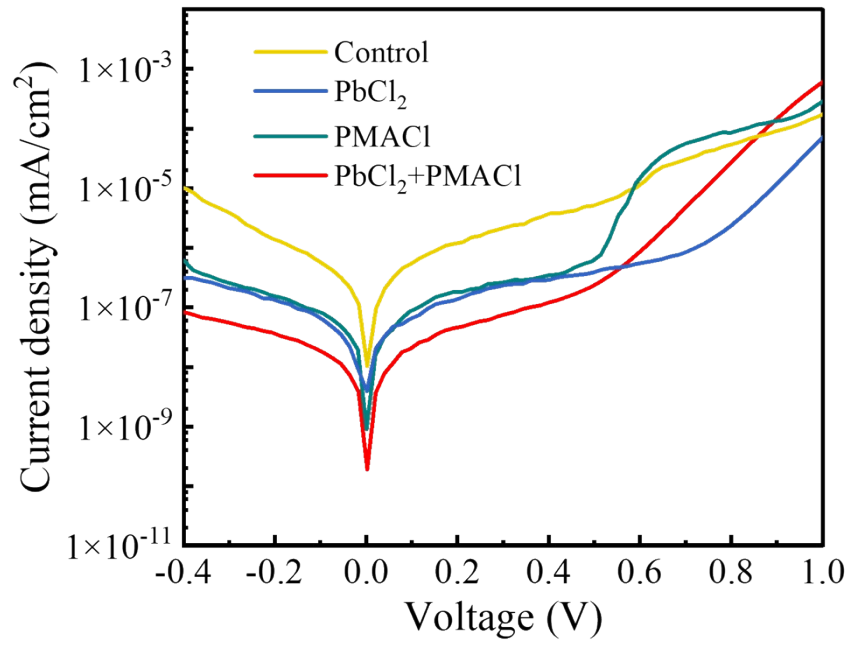
Fig. S25 Dark *J-V* curves of control, PbCl$_2$, PMACl, and PbCl$_2$+PMACl PSCs.
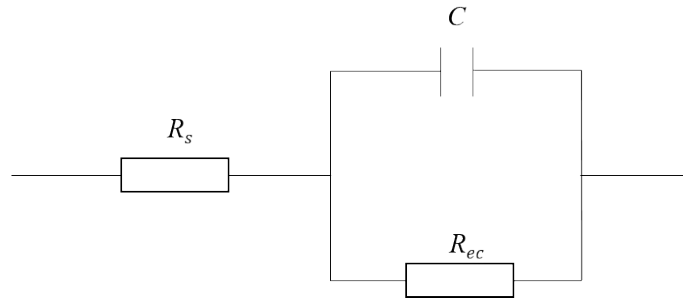
Fig. S26 The equivalent circuit related to the Nyquist plots in Fig. 4d.
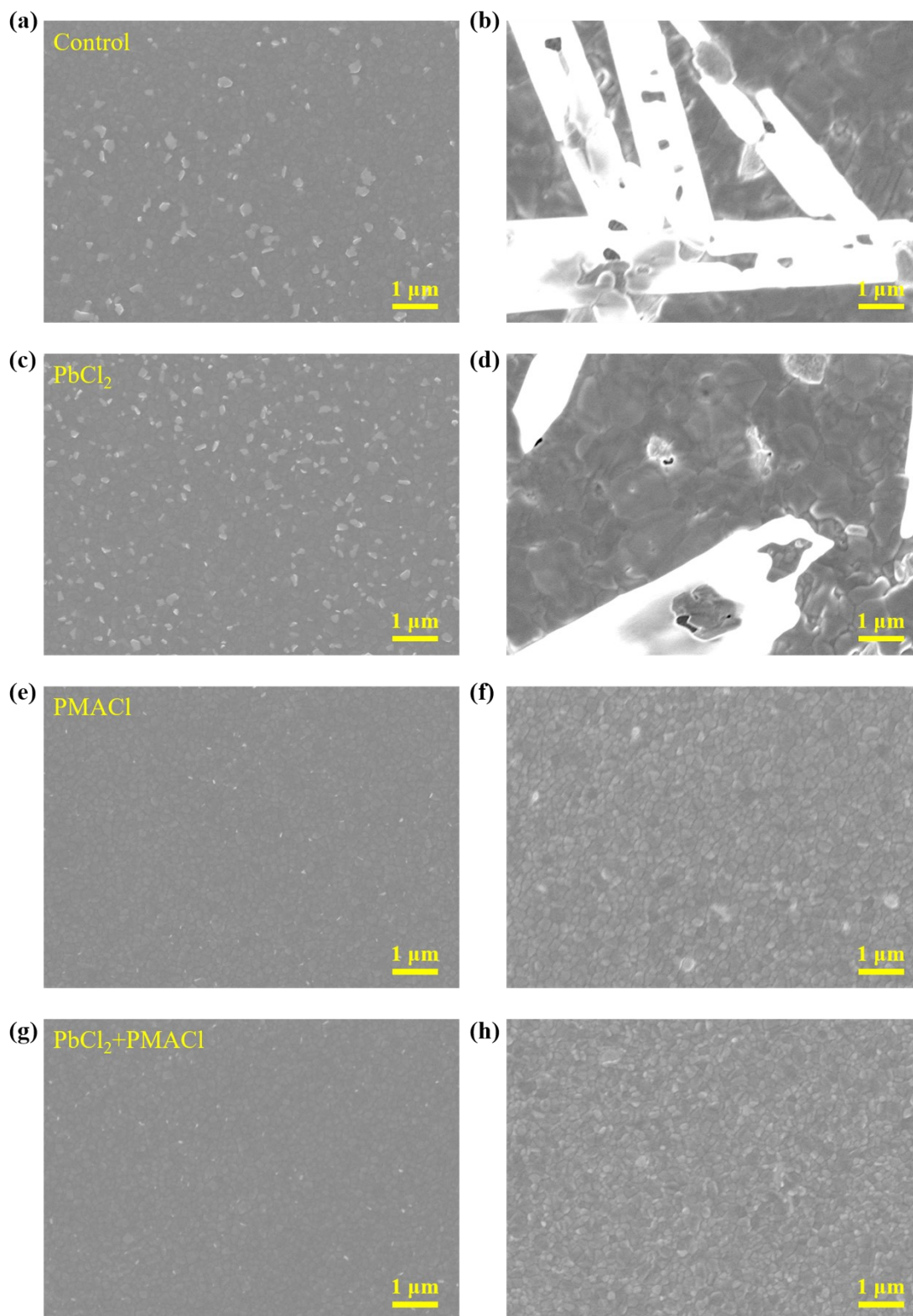
Fig. S27 Top-view SEM images of (a, b) control, (c, d) PbCl$_2$, (e, f) PMACl, and (g, h) PbCl$_2$+PMACl perovskite films. (a), (c), (e), (g) are fresh films, (b), (d), (f), (h) are perovskite films for 180 days under ambient conditions.
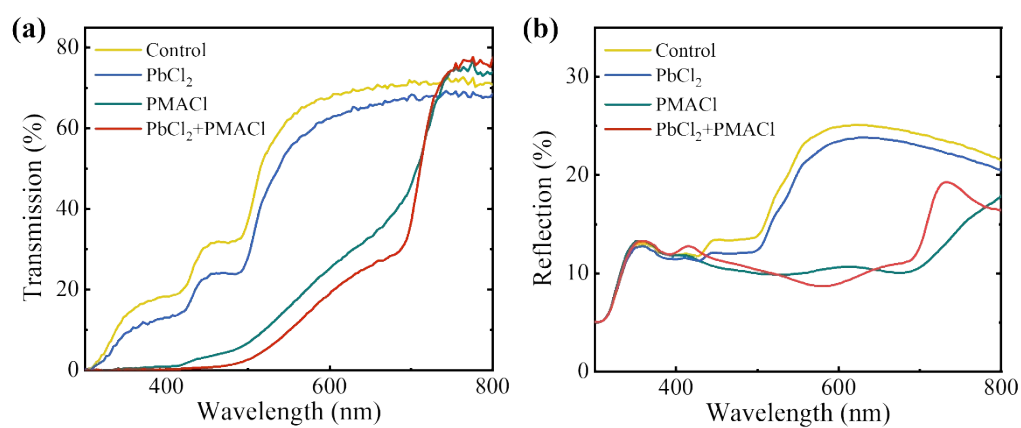
Fig. S28 (a) Transmission and (b) reflection spectra of control, PbCl$_2$, PMACl and PbCl$_2$+PMACl perovskite films exposed in air for 90 days.
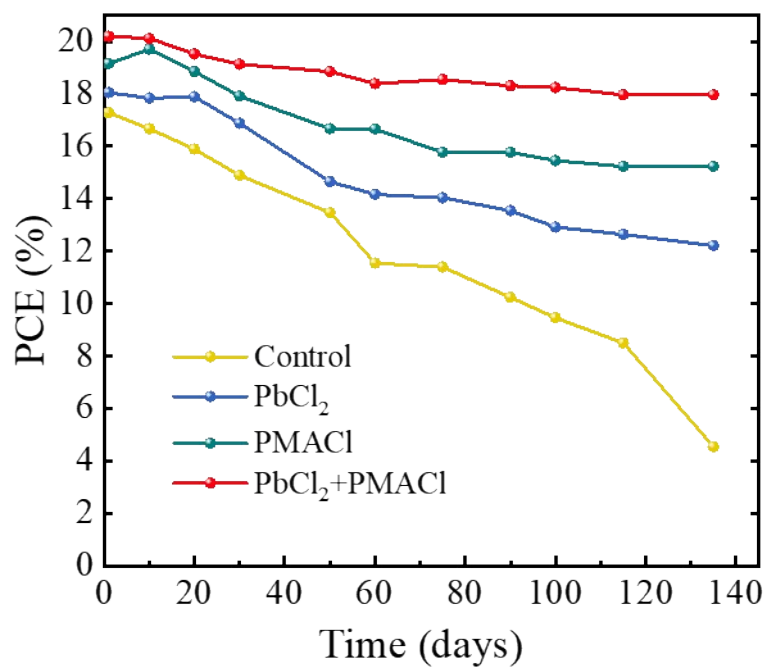
Fig. S29 PCE evolution versus time of PSCs measured in a glovebox for 135 days.
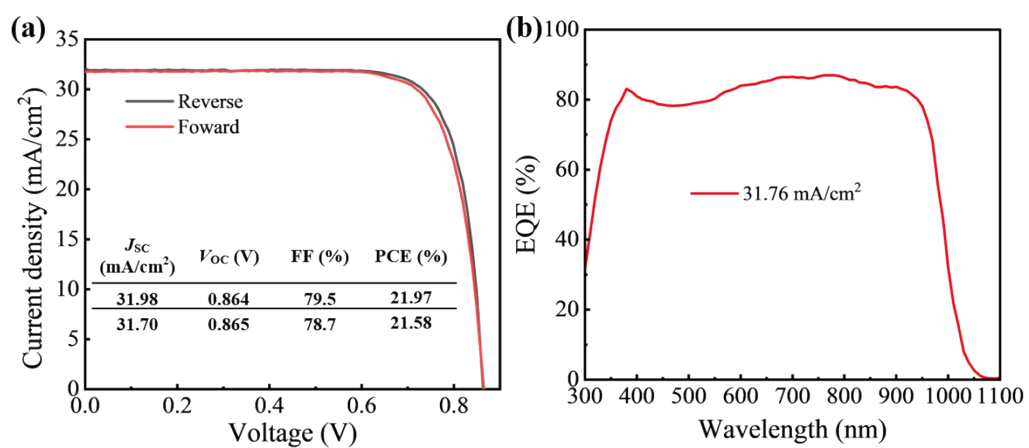
Fig. S30 (a) *J-V* curves under reverse and forward voltage scans, and (b) EQE spectrum of one single-junction low-E_g PSC.

Table S1. Summary on photovoltaic parameters of wide-E_g PSCs with different $PbCl_2$ concentration under 100 mW/cm^2 AM 1.5G illumination measured under reverse voltage scan.

Sample	PCE (%)	V_{OC} (V)	J_{SC} (mA/cm^2)	FF (%)
Control	16.71 ± 0.85	1.164 ± 0.011	17.92 ± 0.35	80.2 ± 2.5
0.5 mol%	17.19 ± 0.28	1.190 ± 0.012	18.03 ± 0.16	80.9 ± 2.3
1.0 mol%	18.05 ± 0.23	1.217 ± 0.016	18.10 ± 0.21	82.0 ± 1.2
1.5 mol%	17.49 ± 1.62	1.203 ± 0.011	18.05 ± 0.22	80.5 ± 7.6
2.0 mol%	17.61 ± 0.72	1.196 ± 0.009	18.02 ± 0.20	81.7 ± 3.1

Table S2. Summary on photovoltaic parameters of wide-E_g PSCs with different PMACl concentration under 100 mW/cm^2 AM 1.5G illumination measured under reverse voltage scan.

Sample	PCE (%)	V_{OC} (V)	J_{SC} (mA/cm^2)	FF (%)
Control	16.71 ± 0.85	1.164 ± 0.011	17.92 ± 0.35	80.2 ± 2.5
0.5 mol%	18.44 ± 0.98	1.256 ± 0.024	18.11 ± 0.98	81.0 ± 1.2
1.0 mol%	18.78 ± 0.98	1.280 ± 0.017	18.05 ± 0.79	81.2 ± 0.8
1.5 mol%	18.67 ± 0.98	1.273 ± 0.013	18.09 ± 0.70	81.0 ± 1.9
2.0 mol%	18.05 ± 0.82	1.269 ± 0.021	17.78 ± 0.77	80.0 ± 1.3

Table S3. Summary on photovoltaic parameters of wide-E_g PSCs with different PbCl$_2$+PMACl concentration under 100 mW/cm^2 AM 1.5G illumination measured under reverse voltage scan.

Sample	PCE (%)	V_OC (V)	J_SC (mA/cm^2)	FF (%)
Control	15.97 ± 1.43	1.167 ± 0.020	17.49 ± 0.77	78.2 ± 3.8
0.5 mol%	18.36 ± 0.91	1.249 ± 0.029	18.10 ± 0.38	81.2 ± 1.7
1.0 mol%	19.26 ± 0.61	1.293 ± 0.025	18.44 ± 0.27	80.8 ± 1.2
1.5 mol%	18.76 ± 0.67	1.278 ± 0.021	18.25 ± 0.26	80.4 ± 2.1

Table S4. Summary on photovoltaic parameters of wide-E_g PSCs with different additives under 100 mW/cm^2 AM 1.5G illumination measured under reverse and forward voltage scans.

Sample	Direction	PCE (%)	V_{oc} (V)	J_{sc} (mA/cm^2)	FF (%)
Control	Reverse	17.38	1.172	18.14	81.7
	Forward	17.16	1.167	17.98	81.7
PbCl$_2$	Reverse	18.19	1.201	18.19	83.2
	Forward	18.14	1.197	18.37	82.5
PMACl	Reverse	19.22	1.278	18.55	81.1
	Forward	19.24	1.267	18.75	81.0
PbCl$_2$+ PMACl	Reverse	20.22	1.312	18.89	81.6
	Forward	20.14	1.310	18.82	81.7

Table S5. Summary on photovoltaic parameters of different additives treated wide-E_g PSCs under 100 mW/cm^2 AM 1.5G illumination measured under reverse voltage scan.

Sample	PCE (%)	V_{OC} (V)	J_{SC} (mA/cm^2)	FF (%)
Control	16.81 ± 0.57	1.167 ± 0.007	17.95 ± 0.40	80.3 ± 1.4
PbCl$_2$	17.83 ± 0.91	1.207 ± 0.022	18.08 ± 0.26	81.9 ± 1.3
PMACl	19.07 ± 0.51	1.280 ± 0.018	18.37 ± 0.56	81.1 ± 0.8
PbCl$_2$+PMACl	19.83 ± 0.53	1.301 ± 0.011	18.75 ± 0.30	81.3 ± 1.2

Table S6. Photovoltaic performance metrics of state-of-the-art inverted wide-E_g PSCs with low V_{OC}-deficits as shown in Fig. 1f.

Year	Type	E_g (eV)	V_{OC}-deficit (V)	V_{OC} (V)	FF (%)	J_{SC} (mA/cm²)	PCE (%)	Ref.
2016	p-i-n	1.75	0.54	1.21	77.9	15.80	14.90	[1]
2016	p-i-n	1.73	0.69	1.04	78.0	15.52	12.59	[2]
2016	p-i-n	1.72	0.56	1.16	78.2	18.3	16.6	[1]
2017	p-i-n	1.71	0.5	1.21	77.5	19.7	18.5	[3]
2017	p-i-n	1.72	0.57	1.15	77.0	19.40	17.20	[4]
2018	p-i-n	1.75	0.53	1.22	73.2	16.30	14.60	[5]
2018	p-i-n	1.68	0.58	1.10	82.0	19.30	17.50	[6]
2018	p-i-n	1.75	0.58	1.17	80.0	17.50	16.30	[6]
2018	p-i-n	1.71	0.47	1.24	77.0	17.45	16.74	[7]
2019	p-i-n	1.77	0.554	1.216	79.7	17.00	16.50	[8]
2019	p-i-n	1.75	0.51	1.24	81.9	17.92	18.19	[9]
2020	p-i-n	1.76	0.555	1.205	81.1	18.55	18.12	[10]
2020	p-i-n	1.75	0.49	1.26	80.0	18.12	18.30	[11]
2020	p-i-n	1.77	0.564	1.206	77.0	17.10	15.90	[12]
2020	p-i-n	1.73	0.48	1.25	78.9	19.48	19.07	[13]
2021	p-i-n	1.70	0.61	1.09	79.0	23.80	20.20	[14]
2021	p-i-n	1.68	0.49	1.19	81.8	20.94	20.31	[15]
2022	p-i-n	1.75	0.511	1.239	81.6	18.20	18.40	[16]
2022	p-i-n	1.79	0.46	1.33	83.9	17.3	19.3	[17]
2022	**p-i-n**	**1.73**	**0.418**	**1.312**	**81.6**	**18.89**	**20.22**	**this work**

Table S7. TRPL parameters of perovskite films with different additives.

Parameter / Sample	τ_1 (ns)	A	τ_2 (ns)	B	τ_{ave} (ns)
Control	28.30	79.44	95.91	20.56	59.89
PbCl$_2$	26.42	69.37	90.70	30.63	65.15
PMACl	25.90	69.85	135.60	30.15	101.94
PbCl$_2$+PMACl	68.92	56.23	257.20	43.77	208.98

The average lifetime (τ) was calculated using the following equation

$$\tau_{ave} = \frac{A\tau_1^2 + B\tau_2^2}{A\tau_1 + B\tau_2}$$

Supplementary References

[1] M. Hu, C. Bi, Y. Yuan, Y. Bai, J. Huang, *Adv. Sci.* **2016**, 3, 1500301.

[2] Z. Yang, A. Rajagopal, S. B. Jo, C. C. Chueh, S. Williams, C. C. Huang, J. K. Katahara, H. W. Hillhouse, A. K. Y. Jen, *Nano Lett.* **2016**, 16, 7739.

[3] Y. Lin, B. Chen, F. Zhao, X. Zheng, Y. Deng, Y. Shao, Y. Fang, Y. Bai, C. Wang, J. Huang, *Adv. Mater.* **2017**, 29, 1700607

[4] X. Zheng, B. Chen, J. Dai, Y. Fang, Y. Bai, Y. Lin, H. Wei, X. C. Zeng, J. Huang, *Nat. Energy* **2017**, 2, 17102.

[5] R. J. Stoddard, A. Rajagopal, R. L. Palmer, I. L. Braly, A. K. Y. Jen, H. W. Hillhouse, *ACS Energy Lett.* **2018**, 3, 1261.

[6] K. A. Bush, K. Frohna, R. Prasanna, R. E. Beal, T. Leijtens, S. A. Swifter, M. D. McGehee, *ACS Energy Lett.* **2018**, 3, 428.

[7] D. B. Khadka, Y. Shirai, M. Yanagida, T. Noda, K. Miyano, *ACS Appl. Mater. Interfaces* **2018**, 10, 22074.

[8] R. Lin, K. Xiao, Z. Qin, Q. Han, C. Zhang, M. Wei, M. I. Saidaminov, Y. Gao, J. Xu, M. Xiao, A. Li, J. Zhu, E. H. Sargent, H. Tan, *Nat. Energy* **2019**, 4, 864.

[9] C. Chen, Z. Song, C. Xiao, D. Zhao, N. Shrestha, C. Li, G. Yang, F. Yao, X. Zheng, R. J. Ellingson, C. S. Jiang, M. Al-Jassim, K. Zhu, G. Fang, Y. Yan, *Nano Energy* **2019**, 61, 141.

[10] Y. Chen, W. Tang, Y. Wu, R. Yuan, J. Yang, W. Shan, S. Zhang, W. H. Zhang, *Solar RRL* **2020**, 4, 2000344.

[11] Z. Li, J. Zhang, S. Wu, X. Deng, F. Li, D. Liu, C. C. Lee, F. Lin, D. Lei, C. C. Chueh, Z. Zhu, A. K. Y. Jen, *Nano Energy* **2020**, 78, 105377.

[12] K. Xiao, R. Lin, Q. Han, Y. Hou, Z. Qin, H. T. Nguyen, J. Wen, M. Wei, V. Yeddu, M. I. Saidaminov, Y. Gao, X. Luo, Y. Wang, H. Gao, C. Zhang, J. Xu, J. Zhu, E. H. Sargent, H. Tan, *Nat. Energy* **2020**, 5, 870.

[13] C. Chen, Z. Song, C. Xiao, R. A. Awni, C. Yao, N. Shrestha, C. Li, S. S. Bista, Y. Zhang, L. Chen, R. J. Ellingson, C.-S. Jiang, M. Al-Jassim, G. Fang, Y. Yan, *ACS Energy Lett.* **2020**, 5, 2560.

[14] F. Sadegh, S. Akin, M. Moghadam, R. Keshavarzi, V. Mirkhani, M. A. Ruiz-Preciado, E. Akman, H. Zhang, M. Amini, S. Tangestaninejad, I. Mohammadpoor-Baltork, M. Graetzel, A. Hagfeldt, W. Tress, *Adv. Funct. Mater.* **2021**, 31, 2102237.

[15] C. Chen, J. Liang, J. Zhang, X. Liu, X. Yin, H. Cui, H. Wang, C. Wang, Z. Li, J. Gong, Q. Lin, W. Ke, C. Tao, B. Da, Z. Ding, X. Xiao, G. Fang, *Nano Energy* **2021**, 90, 106608.

[16] L. Li, Y. Wang, X. Wang, R. Lin, X. Luo, Z. Liu, K. Zhou, S. Xiong, Q. Bao, G. Chen, Y. Tian, Y. Deng, K. Xiao, J. Wu, M. I. Saidaminov, H. Lin, C. Ma, Z. Zhao, Y. Wu, L. Zhang, H. Tan, *Nat. Energy* **2022**, 7, 708.

[17] H. Chen, A. Maxwell, C. Li, S. Teale, B. Chen, T. Zhu, E. Ugur, G. Harrison, L. Grater, J. Wang, Z. Wang, L. Zeng, S. M. Park, L. Chen, P. Serles, R. A. Awni, B. Subedi, X. Zheng, C. Xiao, N. J. Podraza, T. Filleter, C. Liu, Y. Yang, J. M. Luther, S. De Wolf, M. G. Kanatzidis, Y. Yan and E. H. Sargent, *Nature*, **2022**, 611, 278.